European Congress on Computational Methods in Applied Science and Engineering
ECCOMAS 2000
Barcelona, 11-14 September 2000

3D Progressive Damage Analysis of Composites by Combined Finite/Discrete Element Approach

S. Mohammadi[a], D.R.J. Owen[b] and D. Peric[c]

[a] Dept. of Civil Engineering, University of Tehran, Tehran, IRAN
Fax: +98-21-646 1024, Email: smoham@shafagh.ut.ac.ir
[b] Dept. of Civil Engineering, University of Wales Swansea, Swansea, UK
Fax: +44-1792-295676, Email: D.R.J.Owen@swansea.ac.uk
[c] Dept. of Civil Engineering, University of Wales Swansea, Swansea, UK
Fax: +44-1792-295676, Email: D.Peric@swansea.ac.uk

Key words: Progressive Fracture, Discrete Element Method, Delamination, Composite, Impact Loading

Abstract A novel approach, based on the discontinuum concepts of the Discrete Element Method, is presented for fracture and delamination analysis of composites subjected to impact loading. A combined finite/discrete element algorithm is developed for damage analysis of the progressive fracturing and fragmentation behaviour which is observed in composite structures. The algorithm comprises various contact detection and contact interaction schemes to construct an efficient and reliable tool for the modelling of complex post failure phenomena. An anisotropic softening Hoffman failure criterion is adopted for determining the initiation of a crack. The performance of the algorithm is assessed by modelling of a series of engineering applications.

1 Introduction

The idea of using composite materials, in their simplest form, may be traced back to the construction of ancient monuments, where chopped fibrous plants were added to a mixture of mortar and ash to improve its brittleness and to increase its load bearing capacity. Centuries later, the same idea is still being used in the fabrication of advanced composite materials.

Gradually replacing conventional materials, composite laminates are now widely used in many applications involving dynamic loading such as machinery, pressure vessels, defense structures, vehicles, sport equipment and notably aerospace structures [1].

One of the major problems that affects the design and performance of composite materials for structural applications is their vulnerability to transverse impact which may cause substantial internal damage of the component due to matrix cracking, fibre failure and delamination [2].

Figure 1 depicts the progressive fracturing, delamination and fragmentation phenomena in a typical composite specimen subjected to impact loading. This typical representation, is perhaps only relevant to the failure observed in high velocity impact. For low velocity impact, extensive fragmentation is unlikely and material fracture and delamination will be the dominant modes of failure.

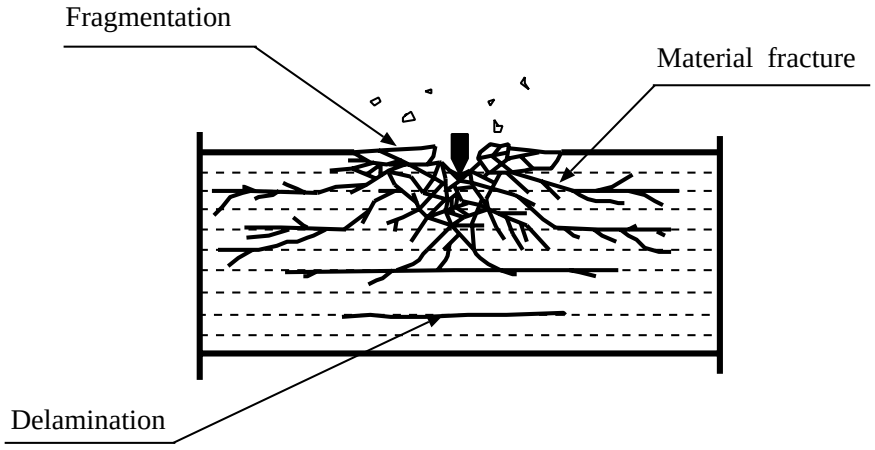

Figure 1: Progressive fracturing, delamination and fragmentation in a typical composite specimen subjected to impact loading.

It should be noted that in a real situation, delamination failure is always accompanied by inplane failures, including matrix and fibre fractures. Therefore a comprehensive study of the behaviour of composites subjected to low or high velocity impacts, requires a

comprehensive scheme which should be capable of modelling progressive in and out of plane fracturing. The treatment of these classes of problems is naturally related to discrete element concepts, in which distinctly separate material regions are considered which may be interacting with other discrete elements through a contact type interaction [3].

In this paper, fundamental aspects of a combined finite/discrete element algorithm for prediction of initiation, propagation and interaction of fracture and delamination phenomena in laminated composites are discribed. In the following, after a general review of the discrete element method, contact interaction formulations will be discussed in detail. Then the crack (material and interlaminar) initiation criteria will be explained and certain numerical issues will be addressed. Several numerical simulations have been performed to assess the performance of the proposed algorithm which covers a variety of benchmark finite element tests, standard experimental data, full scale laboratory tests and practical applications.

2 Discrete element modelling of composites

It has been shown that delamination and material fracture in composites subjected to low or high velocity impact loadings are progressive phenomena which may rapidly propagate throughout the component. This might result in the creation of new totally separated zones, which interact with their surrounding regions. Consequently, a comprehensive scheme is required to monitor the fracturing process and to effectively model both individual and interaction behaviours.

In contrast to the traditional finite element method which is rooted in the concepts of continuum mechanics and is not suited to general fracture propagation problems, the combined finite/discrete element method is specifically designed to solve problems that exhibit strong discontinuities in material and geometric behaviour [4]. The *discrete element method* idealizes the whole medium into an assemblage of individual bodies, which in addition to their own deformable response, interact with each other (through a contact type interaction) to perform the same response as the medium [3].

Consider a composite specimen subjected to an impact loading as depicted in Figure 2. Early material cracks and interlaminar debondings are likely to appear near the position of applied impact load. As the analysis advances, two separate regions can be distinguished. The first one is a highly fractured and delaminated region, and the second is the remainder of the body which contains no delamination or fracture patterns. The predicted fractured/delaminated regions will then be examined in the later stages of the analysis through the developed combined finite/discrete element algorithm. The interface boundaries will be further extended if either the material fracture or the interlaminar debonding has reached the boundaries of the DEM region.

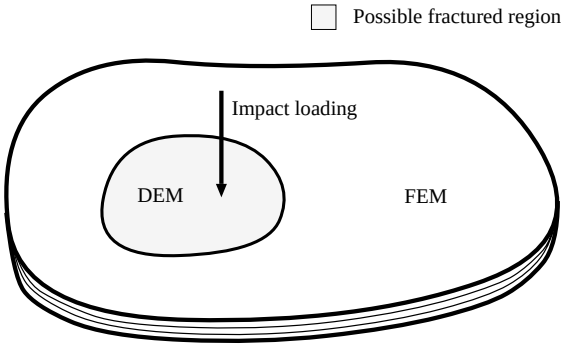

Figure 2: Composite specimen subjected to impact loading.

Figure 3 shows a typical section of the above composite specimen (here, a quarter of the plate). In a combined FE/DE method, the possibly fractured region is modelled using a discrete element mesh and the remainder of the specimen is modelled by a standard finite element mesh. It is also possible to model the whole structure with discrete elements; in which case the possibility of cracking is investigated throughout the structure. A combined mesh enables us to prevent unnecessary contact detection and interaction calculations which comprise a major part of the analysis time.

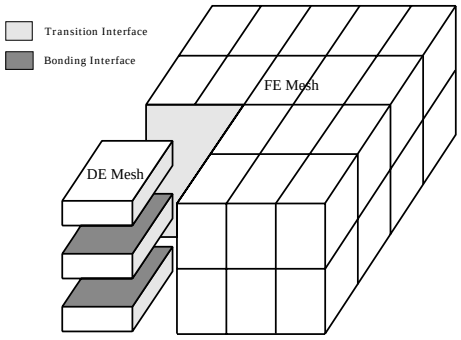

Figure 3: Discrete element modelling of a composite plate.

Each ply or a group of similar plies is modelled by one discrete element. Each discrete element will be discretized by a finite element mesh and may have nonlinear material properties or geometric nonlinearities (large deformations). The interlaminar behaviour of discrete elements is governed by bonding laws, including contact and friction interactions for the post delamination phase.

One important aspect of this type of modelling, which distinguishes it from other contact based delamination algorithms [5, 6], is that it does not require any predefined interface

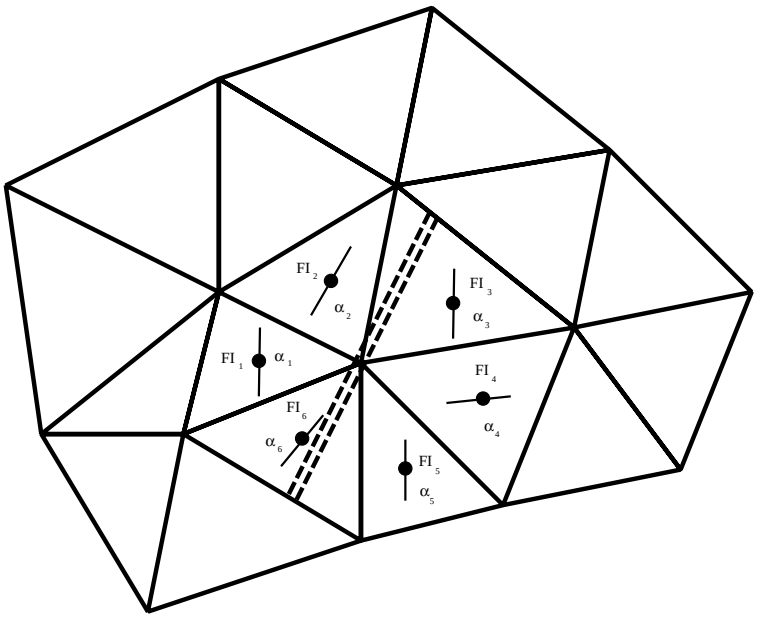

Figure 4: Weighted averaging of the failure indicator and the crack direction for a failed point.

element. Being free from the restrictions of interface elements provides major advantages: Firstly, there is no need for the nodes on different layers to match each other, which eases the way in which data is prepared. This is essential in defining the transition interfaces. Secondly, in progressive cracking, particularly material fracturing, we may end up with new nodes, edges and boundaries that could destroy the compatibility required for these interface elements.

2.1 Remeshing algorithm

Material fracture may result in the creation of new discrete bodies which are in contact by friction interaction with neighbouring bodies. A special remeshing algorithm is adopted to maintain compatibility conditions in newly fractured regions.

The failure indicator and the crack direction for each individual element are evaluated within the material model routines. A weighted averaging scheme is then used to evaluate both the failure indicator and the average crack direction of each node. Figure 4 illustrates this scheme for a two dimensional problem.

The next step is to geometrically simulate the crack and perform the necessary split, separation and the remeshing processes. Figure 5 represents the two dimensional remesh-

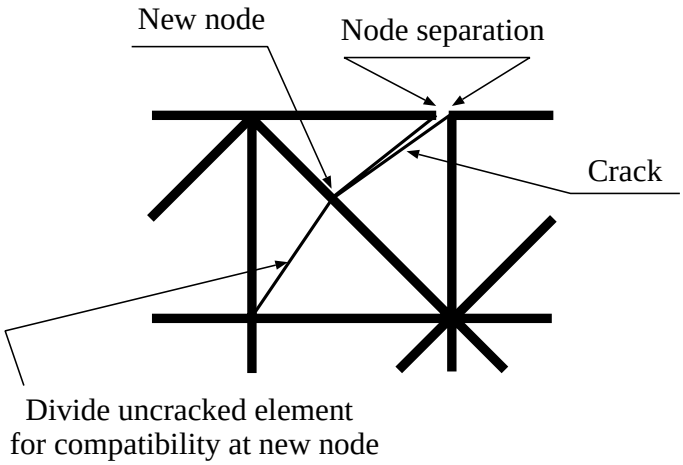

Figure 5: Remeshing scheme for modelling of fracture at a failed point.

ing algorithm which comprises four steps: splitting the element, separating the failed nodes, creating new remeshing nodes, and dividing uncracked elements to enforce compatibility at new nodes. Adopting this local remeshing algorithm will provide a relatively finer mesh in the fractured region and prevents the distortion of the elements in this region, improving the finite element approximation of the analysis.

3 Governing equations

The standard variational (weak) form of the dynamic initial/boundary value problem is taken as the point of departure. Let Ω represent the body of interest and Γ denote its boundary. In a standard fashion the boundary is assumed to consist of a part with prescribed displacement u_i, Γ_{u_i}, and a part with prescribed traction force f_i^{surf}, Γ_{σ_i}. In addition it is assumed that a part Γ_c may be in contact with another body. By denoting

$$\mathcal{V} := \{\delta \boldsymbol{u} : \delta u_i = 0 \quad \text{on} \quad \Gamma_{u_i}\} \tag{1}$$

as the space of admissible variations, the variational form of the dynamic initial/boundary value problem can be expressed as

$$\mathcal{W}^{\text{int}}(\delta \boldsymbol{u}, \boldsymbol{u}) + \mathcal{M}(\delta \boldsymbol{u}, \boldsymbol{u}) = \mathcal{W}^{\text{ext}}(\delta \boldsymbol{u}) + \mathcal{W}^{\text{con}}(\delta \boldsymbol{u}) \tag{2}$$

where

$$\mathcal{W}^{\text{int}}(\delta\boldsymbol{u},\boldsymbol{u}) = \int_{\Omega} \delta\boldsymbol{\epsilon}(\boldsymbol{u}) : \boldsymbol{\sigma}(\boldsymbol{u}) dv \tag{3}$$

$$\mathcal{M}(\delta\boldsymbol{u},\boldsymbol{u}) = \int_{\Omega} \delta\boldsymbol{u} \cdot \rho\ddot{\boldsymbol{u}} dv \tag{4}$$

$$\mathcal{W}^{\text{ext}}(\delta\boldsymbol{u}) = \int_{\Omega} \delta\boldsymbol{u} \cdot \boldsymbol{f}^{\text{body}} dv + \int_{\Gamma_\sigma} \delta\boldsymbol{u} \cdot \boldsymbol{f}^{\text{surf}} da \tag{5}$$

$$\mathcal{W}^{\text{con}}(\delta\boldsymbol{u}) = \int_{\Gamma_c} \delta\mathbf{g}(\boldsymbol{u}) \cdot \boldsymbol{f}^{\text{con}} da \tag{6}$$

denote, respectively, the virtual work of internal forces, the inertial forces contribution, the virtual work of external forces and the virtual work of contact forces. Here $\boldsymbol{\sigma}$ is the Cauchy stress tensor, $\boldsymbol{\epsilon}$ is the strain tensor, $\boldsymbol{u}$ is the displacement vector, while $\mathbf{g}$ represents the contact gap vector. Observe that in the present formulation the contact terms correspond to a penalty formulation of contact interaction.

4 Contact interaction

Once the possibility of contact between discrete elements is detected (by a contact detection algorithm), contact forces have to be evaluated to define the subsequent motion of the discrete elements from the dynamic equilibrium equation. In a penalty method, penetration of the contactor object is used to establish the contact forces between contacting objects at any given time.

To formulate the residual contribution of contact constraint, $\mathbf{r}^c$, for a single boundary node, the component form of the virtual work of the contact forces associated to the contact node is given by:

$$\delta\mathcal{W}^{\text{con}}(\delta\boldsymbol{u}) = f_k^c\, \delta \mathrm{g}_k = f_k^c\, \frac{\partial \mathrm{g}_k}{\partial u_i^s}\, \delta u_i^s \tag{7}$$

where $k = n, t$ and $i = x, y$, and u_i^s is the i-component of the displacement vector at node s, $\mathbf{g} = (\mathrm{g}_n, \mathrm{g}_t)$ is the relative motion (gap) vector, and $\boldsymbol{f}^c$ is the contact force vector over the contact area A^c,

$$\boldsymbol{f}^c = A^c\, \boldsymbol{\sigma}^c \quad , \quad \boldsymbol{\sigma}^c = \boldsymbol{\alpha}\, \mathbf{g} = \begin{bmatrix} \alpha_n & 0 \\ 0 & \alpha_t \end{bmatrix} \begin{bmatrix} \mathrm{g}_n \\ \mathrm{g}_t \end{bmatrix} \tag{8}$$

where $\boldsymbol{\alpha}$ is the penalty term matrix, which can vary for normal and tangential gaps and even between single contact nodes. In theory, larger penalty numbers provide better

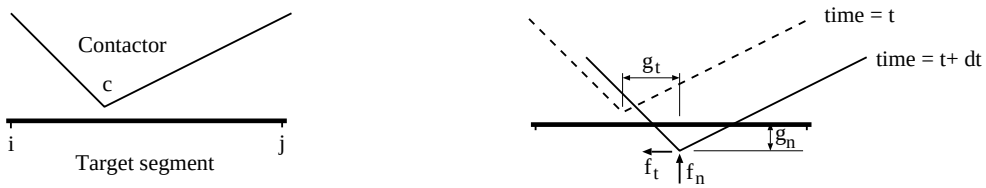

a) Before contact

b) Possible normal and tangential gaps

Figure 6: Normal and tangential gaps.

approximate solutions (better enforcement of the contact constraint), but they may cause numerical instabilities. In fact, α_n and α_t are contact stiffness parameters which are usually evaluated based on the normal and tangential young modulus of the interface (or normal and transverse modulus of the contacting objects), respectively

$$\begin{cases} \alpha_n = (0.5 \sim 2.0)E_n \\ \\ \alpha_t = (0.5 \sim 2.0)E_t \end{cases} \tag{9}$$

The corresponding recovered residual force is then evaluated as:

$$r_i^s = f_k^c \frac{\partial g_k}{\partial u_i^s} \tag{10}$$

The partial derivative part of equation (10) define the direction and distribution of normal and tangential bonding forces.

The possible normal and tangential gaps for each contacting couple are evaluated by monitoring the coordinates of contacting couple nodes in each time step. Then by projecting the coordinates in the current and previous timesteps to a reference configuration, the possible gaps are calculated (Figure 6).

5 Delamination initiation

Figure 7 represents a node to face contact/release algorithm for an interface of two layers during the debonding process. The resultant contact forces over the associated contact area will play the role of required interface stress state to be checked against a delamination criterion.

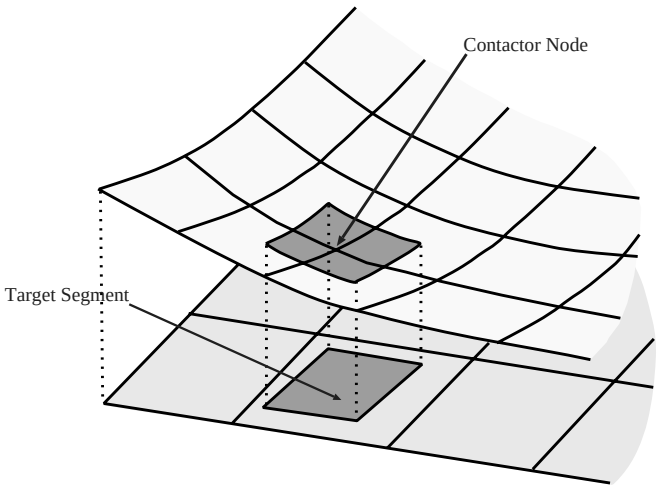

Figure 7: Node to face contact algorithm for delamination interaction.

Several criteria exist that can be used in prediction of the initiation of delamination in composite structures [7, 8]. Reasonable results can be achieved by employing maximum normal stress or strain criteria, but for obtaining more rational results, some other more sophisticated interactive criterion should be adopted. It is widely accepted that the Chang-Springer criterion can be properly used for predicting the initiation of delamination. Three dimensional representation of this criterion in local axes is defined by [9]:

$$(\frac{{\sigma_z}^2}{N^2}) + (\frac{{\sigma_{xz}}^2 + {\sigma_{yz}}^2}{T^2}) = d^2 \begin{cases} d < 1 & \text{no failure} \\ d \geq 1 & \text{failure} \end{cases} \tag{11}$$

where N and T are the unidirectional normal and tangential strengths of the bonding material, respectively.

Once the initial failure is predicted, a further criterion should be introduced to simulate the growth of the local damage as the loading continues.

6 Material model

The imminence of material failure is monitored by the orthotropic Hoffman criterion [10]. According to the Hoffman criterion, a geometric yield surface is constructed from three tensile yield strengths σ_T, three compressive yield strengths σ_C, and three shear yield strengths σ_S. It may be defined as :

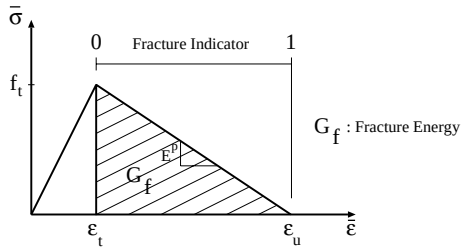

Figure 8: Fracture energy softening model.

$$\Phi = \frac{1}{2}\boldsymbol{\sigma}^T \boldsymbol{P} \boldsymbol{\sigma} + \boldsymbol{\sigma}^T \boldsymbol{p} - \bar{\sigma}^2(\kappa) \tag{12}$$

where the projection matrix $\boldsymbol{P}$, and the projection vector $\boldsymbol{p}$ are defined based on the nine material yield strengths and a normalised yield strength $\bar{\sigma}$ (see Schellekens *et al.* [11]), and κ is a softening/hardening parameter.

7 Crack propagation

Forming a crack is followed by releasing energy and redistributing the forces which caused the initiation of the crack. If this procedure happens immediately after occurrence of a crack, it will lead to inappropriate energy release, and more importantly, to results that strongly depend on the size of the elements used in the analysis.

A bilinear local softening model (the Rankine softening plasticity model) is adopted in this study to account for release of energy and redistribution of forces which caused the formation of a crack. It may properly avoid the mesh dependency of the results by introducing a length scale, l_c, into the softening material model [12].

The fracture energy release is defined as the integral of the area under the softening branch of the stress-strain curve

$$G_f = \left[\frac{1}{2} f_t \left(\epsilon_u - \epsilon_t\right)\right] l_c \tag{13}$$

where f_t is the tensile strength and ϵ_u and ϵ_t are the tensile fracture and ultimate strains respectively, and l_c is the localisation bandwidth. In general, l_c is contained within one

element and, as a close approximation, it may be defined based on the area A, or the volume of the fractured element, V,

$$\begin{aligned} l_c &= A^{\frac{1}{2}} \qquad for\ 2D \\ l_c &= V^{\frac{1}{3}} \qquad for\ 3D \end{aligned} \tag{14}$$

For a bonding check, A is the contact area associated to each contact couple of bonding interfaces (See Figure 7).

The softening modulus is then defined as

$$E^p = \frac{f_t^2\, l_c}{2G_f} \tag{15}$$

8 Numerical simulations

Authors have previously published a number of papers explaining some aspects of the method and verifying the performance of the approach in modelling the complex behaviour of progreeive delamination and fragmentation in composites subjected to impact loadings [12, 13, 14]. Therefore, in this paper only further numerical simulations of some engineering applications are presesnted.

8.1 Fracture and delamination buckling analysis of an orthotropic composite beam

Two orthotropic composite specimens with different laminate layouts are considered. Each laminate is composed of T300/976 graphite epoxy prepreg tape (See Table 1 [7]). The composite $[90_n, 0_n, 90_n]$ and $[0_n, 90_{2n}, 0_n]$ ply layouts are assigned to the beams with $(LHW = 10.16, 0.249, 2.54cm)$ and $(LHW = 7.62, 0.228, 2.63cm)$ geometric descriptions, respectively. The specimens are subjected to quasi-static concentrated loading $(P = 2300\, KN)$ applied at their centre lines. Eight and nine layer finite/discrete element meshes were used to model half of the beams, respectively.

Figures 10a,c illustrate the buckling modes of delaminated layers for both beams. Liu *et al* [7] reported the same delamination patterns at the interface of the bottom $[0_n]$ and $[90_n]$ plies for the $[0_n, 90_{2n}, 0_n]$ specimen. However, no buckling mode was reported at the top delaminated interface for the $[90_n, 0_n, 90_n]$ specimen (See Figure 9).

In addition to a delamination analysis, a fracture analysis was performed to predict the real damage modes of the beams (Figure 10b,d). Matrix cracking across the thickness

Table 1: Material properties of the orthotropic composite beam.

$E_{xx} = 139200MPa$	,	$G_{xx} = 5580MPa$
$E_{yy} = 9700MPa$	,	$G_{yz} = 3760MPa$
$\nu_{xy} = \nu_{yz} = 0.3$	,	$\rho = (1.38 - 2)\frac{Mg}{m^3}$
$X_t = 1150MPa$	,	$X_c = 1120MPa$
$Y_t = 40MPa$	,	$Y_c = 170Mpa$
$S = 100MPa$		

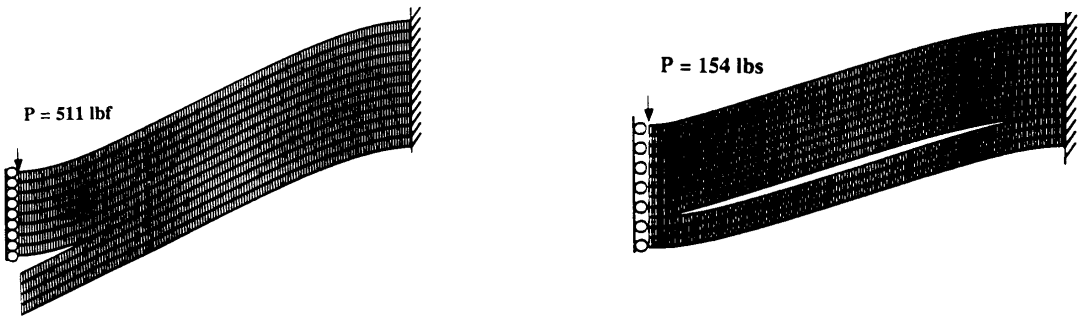

(a) $[90_n, 0_n, 90_n]$ layout.

(b) $[0_n, 90_{2n}, 0_n]$ layout.

Figure 9: Deformed shape of composite specimens reported by Liu *et al* [7].

of the top layer of the first specimen prevents the formation of a buckling mode and the overall behaviour of the specimen reduces nearly to an unbonded multi-layer beam.

The fracture patterns for the second specimen are mainly concentrated within the weak mid layer of the beam, specially around the loading region, while extensive delaminations are formed at the interfaces of $[90_n]$ and $[0_n]$ layers.

8.2 Impact loading of a composite plate - delamination analysis

A numerical simulation is undertaken to assess the performance of the method for dealing with progressive debonding phenomenon in a laminated composite plate which is subjected to a high velocity impact at its centre. Because of symmetry, only one quarter

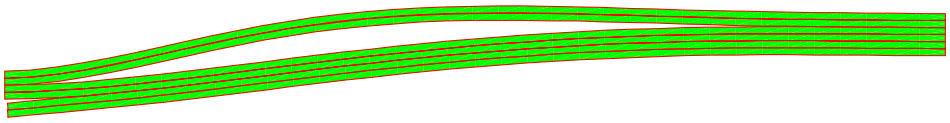

(a) Buckling of top delaminated layer

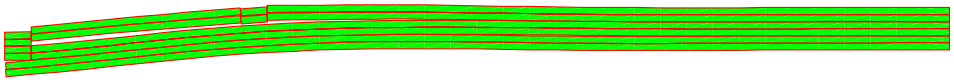

(b) Fracture patterns.

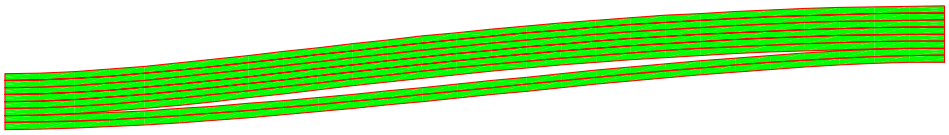

(c) Delamination patterns.

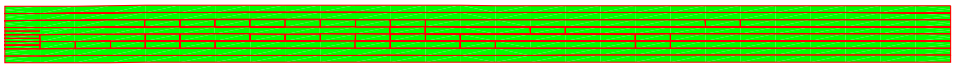

(d) Fracture patterns.

Figure 10: Deformed shape and crack patterns of composite specimens. a,b)$[90_n, 0_n, 90_n]$ layout, c,d)$[0_n, 90_{2n}, 0_n]$ layout.

of the plate is modelled. Also, only the central region of this model is meshed by a DE mesh. Therefore, the possibility of delamination is only investigated in this region (See Figure 11). Material properties and other necessary information are given in Table 2 [15]. The composite ply pattern is set to $[90_n, 0_n, 90_n, 0_n, 90_n]$. This modelling is a numerical simulation of the experiments undertaken by Worswick et al. [15] on evaluating impact damage on composite plates. The impact loading is simulated by a triangular load applied from 0 to 5 μsec with a variable peak force of 1 to 5 kN for different tests. In this analysis, the peak loading is set to 5 kN.

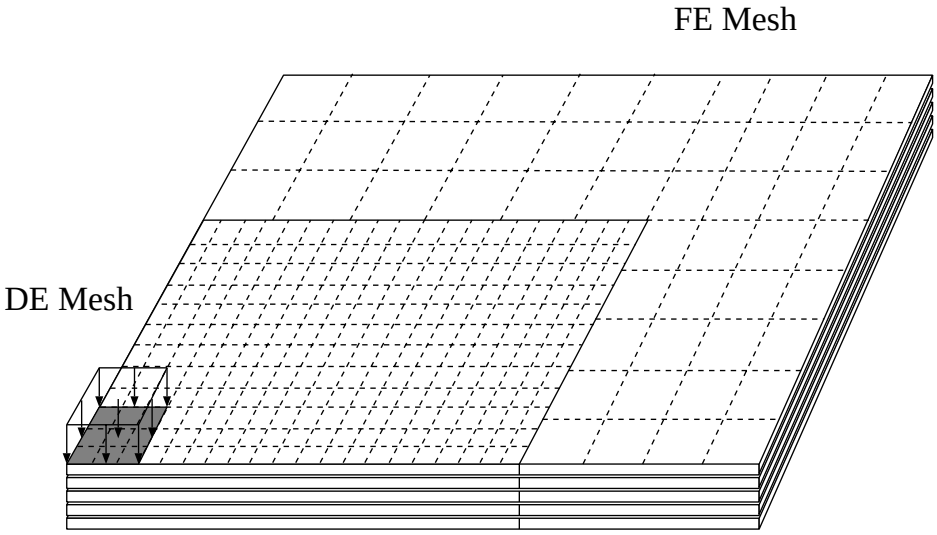

Figure 11: FE/DE mesh of the composite plate. (del. only)

Figures 12 to 13 illustrate the debonding patterns at different layer interfaces for two different stages of the loading. Delamination patterns are clearly developing from the central region of the plate, i.e. the impacted zone, towards the edges of the plate. These figures depict only the DE part of the whole mesh.

Figure 14 depicts the comparison of the displacement history of the centre of the plate for this mesh and a coarser mesh. The comparisons are made for both the top and bottom point across the thickness of the plate, and clearly shows the mesh independency of the results.

It should be noted that these results were achieved without considering a material fracture analysis, and only the bonding fracture was activated. In a practical test, however, the illustrated large deformation will certainly involve extensive material fracture.

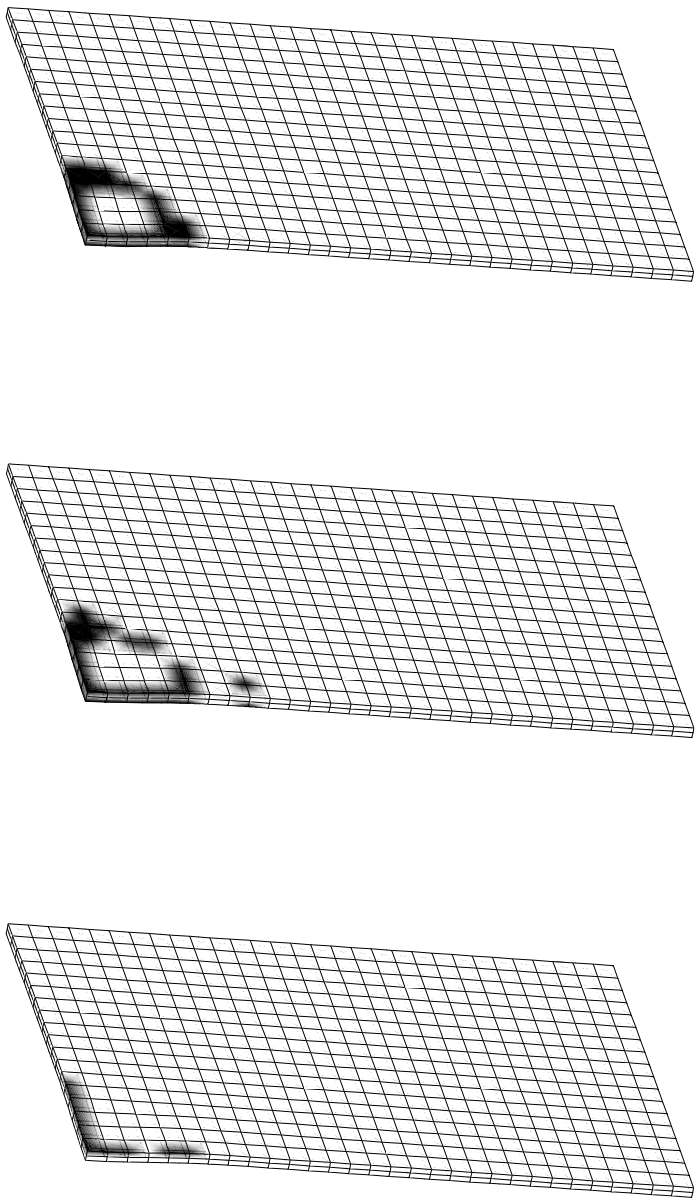

Figure 12: Delamination patterns at layer interfaces at T=0.00006 sec.

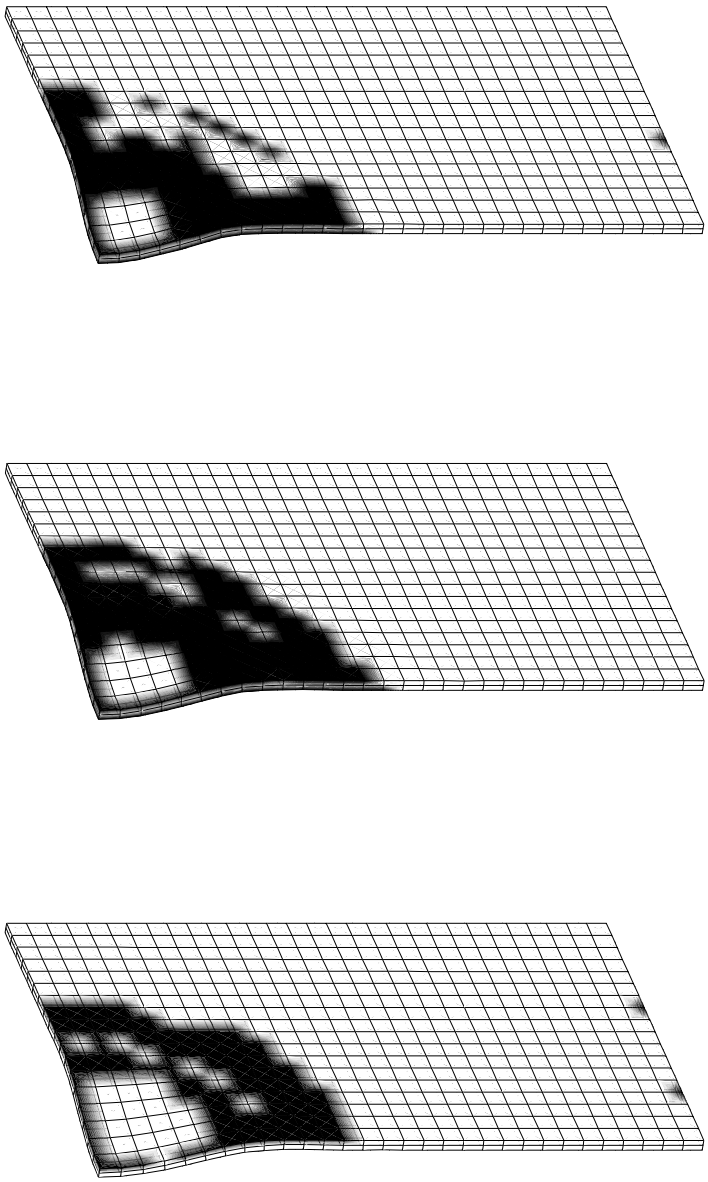

Figure 13: Delamination patterns at layer interfaces at T=0.00012 sec.

Table 2: Material properties for T800/P2302-19 graphite resin.

Model size $= 0.0762 \times 0.0508 \times 0.00444m$
DE region $= 0.050 \times 0.035m$
Ply layout $[90, 0, 90, 0, 90]$
$E_{xx} = 152.4e3MPa$, $E_{yy} = 10.7e3MPa$
$\nu = 0.35$, $\rho = 1.55e3\frac{Kg}{m^3}$
$X_t = 2772MPa$, $X_c = 3100.0MPa$
$Y_t = 79.3MPa$, $Y_c = 231.0MPa$
$S = 132.8MPa$

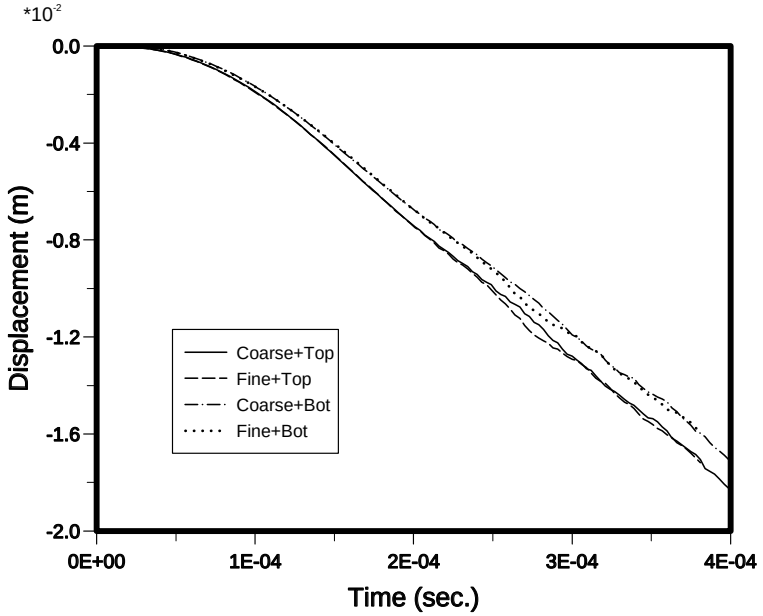

Figure 14: Comparison of the displacement history of the central point for coarse and fine meshes at the top and bottom point of the thickness.

9 Conclusions

The combined finite/discrete element has proved to be an efficient algorithm for dealing with multi-fracture and fragmentation processes, which frequently arise from impact loadings on composite structures. It is also shown that the delamination behaviour in composite specimens can be effectively modelled by this method. The algorithm comprises various contact detection and contact interaction schemes to construct an efficient and reliable tool for the modelling of complex post failure phenomena. In addition to considering the potential pre-delamination contacts, it is also essential to take into account the contact and friction interactions for post debonding or fracture behaviour of composites. A major advantage of the method is that it does not require any predefined interface elements, which are considered inappropriate for efficient computational modelling of combined progressive multi-fracture and delamination analysis.

An anisotropic softening Hoffman failure criterion is adopted for specifying the initiation of a crack. A local remeshing scheme is introduced for geometric modelling of the cracks, which plays an important role in avoiding the excess distortions of the finite elements in the vicinity of cracks. The algorithm allows for both nodal separation and splitting a cracked element. The imminence of a bonding crack is predicted by the Chang-Springer criterion. A bilinear softening model is adopted for both matrix and interlaminar cracking description to prevent the mesh dependency of the results.

10 Acknowledgements

The first author would like to acknowledge the support received from the University of Tehran and the Ministry of Culture and Higher Education of I.R. IRAN.

References

[1] C.G. Koh, D.R.J. Owen, and D. Peric. Explicit dynamic analysis of elasto-plastic laminated composite shells: implementation of non-iterative stress update schemes for the hoffman yield criterion. *Computational Mechanics*, **16**:307–314, 1995.

[2] F.L. Matthews and R.D. Rawlings. *Composite Materials : Engineering and Science*. Chapman and Hall, 1994.

[3] N. Bicanic, A. Munjiza, D.R.J. Owen, and N. Petrinic. From continua to discontinua - a combined finite element / discrete element modelling in civil engineering. In B.H.V.

Topping, editor, *Developments in Computational Techniques for Structural Engineering*, pages 1–13. Civil-Comp Press, 1995.

[4] A. Munjiza, D.R.J. Owen, and N. Bicanic. A combined finite-discrete element method in transient dynamics of fracturing solids. *Engineering Computations*, **12**:145–174, 1995.

[5] Y. Mi, M.A. Crisfield, and G.A.O. Davies. Failure modelling in composite structures. In M.A. Crisfield, editor, *Computational Mechanics in UK - 5th ACME Conference*, pages 36–39, April 1997. London, UK.

[6] X. Zhang, D. Hitchings, and G.A.O. Davies. Modelling composite failure and delamination during low velocity impact. In M.A. Crisfield, editor, *Computational Mechanics in UK - 5th ACME Conference*, pages 44–47, April 1997. London, UK.

[7] S. Liu, Z.Kutlu, and F.K.Chang. Matrix cracking-induced delamination propagation in graphite/epoxy laminated composites due to a transverse concentrated load. In W.W. Stinchcomb and N.E.Ashbangh, editors, *Composite Materials : Fatigue and Fracture, ASTM STP 1156*, volume **4**, pages 86–101, 1993.

[8] V. Tvergaard. Effect of fiber debonding in a whisker-reinforced metal. In *Materials Science and Engineering A : Structural Materials : Properties, Microstructure, and Processing*, volume A125(2), pages 203–213, June 1990.

[9] F.K. Chang and G.S. Springer. The strength of fiber reinforced composite bends. *Composite Materials*, **20**(1):30–45, 1986.

[10] R.E. Rowlands. Strength (failure) theories and their experimental correlation. In G.C. Sih and A.M. Skudra, editors, *Handbook of Composites, Vol. 3 - Failure Mechanics of Composites*, chapter 2, pages 71–125. Elsevier Science Publishers B.V., 1985.

[11] J.C.J. Schellekens and R. de Borst. The use of hoffman yield criterion in finite element analyses of anisotropic composites. *Computers and Structures*, **37**(6):1087–1096, 1990.

[12] S. Mohammadi, D.R.J. Owen, and D. Peric. Delamination analysis of composites by discrete element method. In D.R.J. Owen, E. Onate, and E. Hinton, editors, *Computational Plasticity, COMPLAS V*, pages 1206–1213, March 1997. Barcelona, Spain.

[13] D.R.J. Owen, D. Peric, and S. Mohammadi. Discrete element modelling of multi-fracturing solids and structures. In *Foreign Object Impact and Energy Absorbing Structure*, pages 47–64. Institution of Mechanical Engineers (IMechE), Aerospace Industries Division, March 1998. London.

[14] S. Mohammadi, D.R.J. Owen, and D. Peric. A combined finite/discrete element algorithm for delamination analysis of composites. *Finite Elements in Analysis and Design*, **28**:321–336, 1998.

[15] M.J. Worswick, P.V. Strazincky, and O. Majeed. Dynamic fracture of fiber reinforced composite coupons. In C.T.Sun, B.V. Sankar, and Y.D.S. Rajapakse, editors, *Dynamic Response and Behaviour of Composites*, ASME AD-Vol. 46, pages 29–41, 1995.